

Two-stage Adaptive Restoration Decision Support System for a Self-healing Power Grid

Amir Golshani, *Student Member, IEEE*, Wei Sun, *Member, IEEE*, Qun Zhou, *Member, IEEE*, Qipeng P. Zheng, *Member, IEEE*, and Jianzhong Tong, *Fellow, IEEE*

Abstract—Power outages cost American industries and businesses billions of dollars and jeopardize the lives of hospital patients. The losses can be greatly reduced with a fast, reliable and flexible self-healing tool. This paper is aimed to tackle the challenging task of developing an adaptive restoration decision support system (RDSS). The proposed RDSS determines restoration actions both in planning and real-time phases and adapts to constantly changing system conditions. The comprehensive formulation encompasses practical constraints including AC power flow, dynamic reserve, and load modeling. The combinatorial problem is decomposed into a two-stage formulation solved by an integer L-shaped algorithm. The two stages are then executed online in the RDSS framework employing a sliding window method. The IEEE 39-bus system has been studied under normal and contingency conditions to demonstrate the effectiveness and efficiency of the proposed online RDSS.

Index Terms—Adaptive restoration, dynamic reserve, integer L-shaped algorithm, mixed-integer linear programming, two-stage optimization.

I. NOMENCLATURE

Decision variables:

$u_{on}^{i,t}$	Binary variable equal to 1 if unit i is on at time t .
$u_{start}^{i,t}$	Binary variable equal to 1 if unit i is in a start-up period at time t .
t_{start}^i	Start-up time of unit i .
$P_g^{i,t}$	Scheduled real power of unit i at time t after connecting to the grid.
$P_{gstart}^{i,t}$	Start-up power of unit i at time t .
$u_{bus}^{b,t}$	Binary variable equal to 0/1 if bus b is de-energized/energized at time t .
$u_{line}^{nm,t}$	Binary variable equal to 0/1 if the line between buses n and m is de-energized/energized at time t .
$q_+^{i,t}, q_-^{i,t}$	Positive and negative fictitious reactive power at bus i and time t .

This work is supported in part by the U.S. National Science Foundation under Grant ECCS-1552073 and Grant CMMI-1355939, and AFRL Mathematical Modeling and Optimization Institute.

A. Golshani, W. Sun, and Q. Zhou are with the Department of Electrical and Computer Engineering, University of Central Florida, Orlando, FL, 32816 USA. (e-mail: amir.golshani@knights.ucf.edu, sun@ucf.edu, qun.zhou@ucf.edu.)

Q. P. Zheng is with the Department of Industrial Engineering and Management Systems, University of Central Florida, Orlando, FL, 32816 USA. (e-mail: qipeng.zheng@ucf.edu.)

J. Tong is with the PJM interconnection L.L.C., PA 19403 USA. (e-mail: jianzhong.tong@pjm.com)

Copyright (c) 2009 IEEE. Personal use of this material is permitted. However, permission to use this material for any other purposes must be obtained from IEEE by sending a request to pubs-permissions@ieee.org.

$P_{load}^{l,t}, Q_{load}^{l,t}$	Amount of real and reactive loads restored at load bus l and time t .
$P_f^{nm,t}, Q_f^{nm,t}$	Real and reactive power flows between buses n and m at time t .
$V^{n,t}, \theta^{n,t}$	Voltage amplitude and angle of bus n at time t .
$y^{nm,t}$	Piecewise linear approximation of $\cos(\theta^n - \theta^m)$ at time t .
$\Delta P_{max}^t, \Delta P_{max}^{i,t}$	Total load pickup capability and load pickup capability of unit i at time t .
$P_{reserve}^{dyn,t}, P_{reserve}^{dyn,i,t}$	Total dynamic reserve and dynamic reserve share of unit i at time t .
$P_{shed}^{l,t}$	Load shedding share of load bus l at time t .
ΔP_{CLPU}^t	Impact of cold load pickup at restoration time t .
$Q(x), \phi$	Second-stage objective function and estimated second-stage objective function.
$P_{load}^{max,l,t}, Q_{load}^{max,l,t}$	Maximum restorable active and reactive loads at load bus l and time t .

Constant parameters:

$P_g^{max,i}, P_g^{min,i}$	Maximum and minimum real power capacities of unit i .
$Q_g^{max,i}, Q_g^{min,i}$	Maximum and minimum reactive power capacities of unit i .
P_{gstart}^i	Cranking power of unit i .
α_l, β_l	Priority factor and cold load percentage of load l .
pfl, λ_l	Power factor at load bus l and additional power demand caused by cold load pickup.
$T_{start}^i, \hat{t}_{start}^i$	Start-up duration of unit i and start-up time of unit i calculated at $t = 0$.
M	Large positive number.
μ_z, μ_I, μ_p	Coefficients of constant impedance, constant current and constant power loads.
V^{min}, V^{max}	Minimum and maximum limits of voltage.
g_{nm}, b_{nm}, b_{nm}^c	Conductance, susceptance, and shunt susceptance of the transmission line between buses n and m .
\hat{R}_g, \hat{M}^t	Total ramping rate and total inertia of all online generation units at time t .
f_{min}, f_{db}, f_0	Minimum allowable frequency, governor's dead band and nominal frequency.
N_r	Number of segments in cosine function

$\hat{Q}_{load}^{tot,t}$	approximation.
$\hat{Q}_{ch}^{nm,t}, \hat{Q}_{loss}^{nm,t}$	Total restored reactive load at time t . Reactive charging power and reactive power loss of the line between buses n and m at time t .
$\hat{S}^{nm}, \hat{P}^{nm}$	Apparent power limitation and active power loss limit of line nm .
D	Iteration count in integer L-shaped algorithm.
Sets:	
L_{CLPU}, L	Sets of load buses containing cold loads and set of load buses.
T, T'	Sets of restoration times before and after the contingency.
L_{sh}	Set of load buses with under-frequency load shedding relays.
I, I_{BSU}, I_{NBSU}	Sets of generators, black-start units, and non-black-start units.
B, K	Sets of buses and transmission lines.
I_{in}, B_{in}, K_{in}	Sets of generators, buses, and transmission lines that are not affected by the contingency.
$I_{out}, B_{out}, K_{out}$	Sets of generators, buses, and transmission lines that are affected by the contingency.
Indices:	
n, m, b	Indices for system buses.
i, l, t, b_i, b_l	Indices for generation units, loads, times, generator buses, and load buses.
t, t'	Indices for times before and after contingency.

II. INTRODUCTION

LARGE power outages become more common place due to the increase in both frequency and strength of natural disasters and cyber-attacks. For instance, in 2012, hurricane Sandy devastated the power grid along the east coast of the U.S., leaving more than 8 million people without power for over a week. In addition to such massive destructions due to natural disasters, partial blackouts usually occur as a result of damage to a local utility infrastructure or cyber attacks. Furthermore, as the electricity demand is growing over time, power systems are operating under stressed conditions which reduces the security margin and increases the likelihood of cascading outages [1]. According to the Electric Power Research Institute, across all business sectors the U.S. economy loses over 150 billion dollars a year due to power outages [2]. To reduce the loss and enhance resiliency, a fast and reliable power system self-healing tool with integration of newer and more intelligent technologies is critically needed.

System operators are currently guided by a series of restoration plans prepared offline based on a set of blackout scenarios [3], [4]. Major independent system operators (ISOs) in the U.S., such as Pennsylvania-New Jersey-Maryland (PJM) interconnection and ISO New England, provide restoration manuals to guide operators in disturbance conditions or after a blackout [5], [6]. Offline restoration plans are developed

to assist system operators to bring the power back after a major blackout. However, the offline restoration plans need to be constantly checked against system conditions. As a result, system recovery is prolonged and system operators face tremendous pressure. Moreover, unexpected events can occur during the restoration process, e.g., loss of generation or transmission lines, imposing further challenges in restoration.

Much research efforts have been devoted to the self-healing actions in power grid, particularly, in restorative state [7]-[20]. Authors developed a decision support system for generating an optimal black-start strategy in [7]. This system contains mixed-integer nonlinear optimization programming (MINLP) problem which is difficult to solve by traditional optimization techniques. Also, it currently serves as an offline planning tool in Taiwan power company. In [8] and [9], authors applied the expert system functions in power system restoration and proposed the use of analytical tool without presenting any mathematical formulations. An online decision support tool together with the concept of generic restoration milestones (GRMs) was discussed in [10]. In the proposed method, several optimization problems representing different restoration stages need to be solved separately which increased the complexity of this approach, particularly for online applications.

Our prior work has developed a mixed-integer linear programming (MILP) algorithm to maximize overall generator start-up capability [11]. However, that work only considered the generation start-up problem without formulating other phases of restoration process. In [12], a transmission path selection method was proposed to restore the de-energized loads. Authors adopted the power transfer distribution factor matrix to calculate the power flow on the restored lines. However, that work mostly emphasized the correct sequence of transmission line energization by defining two indices, with limited insights on the whole restoration problem. Restoration for interconnected power systems was proposed using tie-lines and collaboration among transmission system operators (TSOs) [13]. This collaboration leads to the optimal allocation of the available cranking sources to non-black-start units. However, a simplified load pickup increment approach was suggested which does not accurately reflect the generation units characteristics.

For load restoration, a wide-area measurement system (WAMS)-based approach was introduced in [14]. And a two-stage transmission-level load restoration based on synchrophasor data was also been proposed in [15]. In both references authors only studied the final phase of restoration process, when all generation units are on and transmission lines are energized. Reference [16] paid particular attention to the load restoration phase considering generator start-up constraints. However, it simply approximated the load pickup step calculation and cannot adapt to changing operating conditions. Combined restoration optimization problem was solved using Firefly algorithm in [17]. Generally, metaheuristic methods are trapped in local minima and do not guarantee the global optimality of solutions. Also, the proposed approach did not consider power flow equations, and was only suggested for the planning phase of restoration. In [18], it was shown that DC power flow model is not sufficiently accurate for

solving the restoration problem. To overcome this issue, it proposed a linear programming approximation of AC power flow considering reactive power and voltage magnitudes.

In distribution network, service restoration under contingencies has been studied in [19] and [20]. Distribution system restoration with plug-in hybrid electric vehicles (PHEVs) and storages was investigated in [19]. Particularly, the impact of parking lots on restoration process was examined under contingency cases. The proposed healer reinforcement approach was tested on the radial network structure. A multiagent-based distribution restoration under both single and multiple recurring faults was explored in [20]. However, network loss, voltage and current limitations, and load priorities have not been incorporated in the service restoration problem.

In summary, a transmission system restoration tool that can combine different phases of restoration process into a single optimization problem, respond to the changing conditions and contingencies, and being computationally efficient for both planning and real-time cases is lacking in the literature. To address the aforementioned shortages, our paper presents a holistic adaptive restoration decision support system (RDSS) by formulating a two-stage mixed-integer linear optimization problem. The approach presented in this paper adapts to changing operating conditions in restoration. The proposed RDSS serves as a crucial component for the future self-healing power grid. Our major contributions are summarized as follows.

- 1) The proposed RDSS integrates different phases of restoration into one holistic problem. The RDSS looks ahead over the entire restoration time horizon to ensure global optimality with the shortest restoration time. It contains various practical constraints including generators' start-up times, line energization sequences, AC load flow, load pickup and dynamic reserve constraints.
- 2) The proposed RDSS is computationally fast for real-time operation. In this paper, we propose an efficient decomposition approach based on the integer L-shaped algorithm with a novel integer L-shaped cut. The two stages are then executed using a sliding window framework which only requires to solve the second-stage problem in real-time unless a major event occurs.

The remainder of this paper is organized as follows. Section III describes the RDSS framework. Section IV presents the problem formulations with objectives and constraints before and after the contingency. The solution methodology is described in Section V. Section VI presents numerical results to demonstrate the effectiveness and efficiency of the proposed RDSS. Conclusions drawn from this work are presented in section VII.

III. RDSS FRAMEWORK

Power system restoration is a complex nonlinear problem containing different phases, variables and constraints. Restoration tasks are performed by starting a black-start unit (BSU), finding transmission paths to crank non-black-start units (NB-SUs) and serving critical loads. The proposed RDSS combines these stages into one holistic problem, and then decomposes

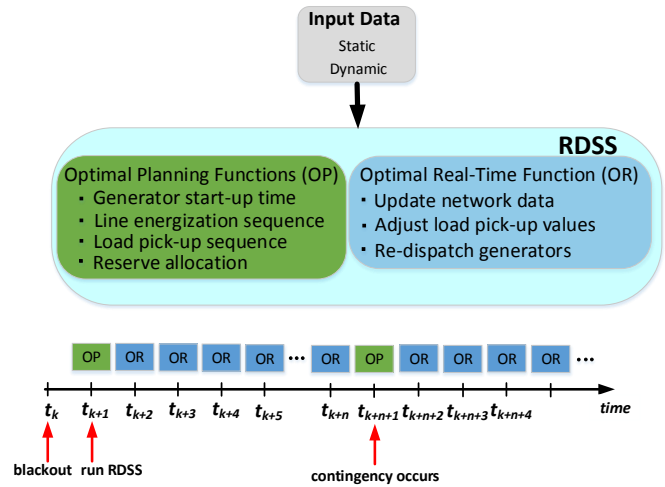


Fig. 1. Proposed RDSS framework and application in restoration period.

into a two-stage problem formulation. The two-stage problem is then executed with a sliding window by looking ahead over the entire restoration time horizon. Therefore, the performance is greatly enhanced so that the RDSS can be utilized in a real-time environment.

The proposed RDSS contains two types of functions: optimal planning (OP) and optimal real-time (OR) functions, with each of them executed at specific time periods, as shown in Fig. 1. The OP function is executed right after the blackout at t_{k+1} , while the OR function is run periodically at each restoration time step. The RDSS has static and dynamic input data. Static inputs include power system topological information such as transmission and generator parameters. Dynamic inputs are system states that are updated in real-time with data from phasor measurement units (PMUs) or supervisory control and data acquisition (SCADA) systems. With the initial outage conditions such as generation units and transmission lines availability, system operators run the RDSS to determine the optimal restoration plan. The results obtained from the OP stage provides a step-by-step restoration action list. This list contains the starting times of all generators, energization times of all buses and lines, the optimal location and amount of loads to pickup, and the amount of dynamic reserve to ensure system security.

As restoration process proceeds, more generating units, transmission lines and loads become online, leading to the changes of system dynamic characteristics. These changes are mostly related to the load pickup capability and dynamic reserve provision. And they are directly affected by governors' responses, characteristics of the loads, and total system inertia. However, the decision variables pertaining to generators' start-up and buses/lines energization times, whose values were determined after solving the OP problem at t_{k+1} , can be assumed to remain unchanged. Having these binary decision variables determined, OR function is run every few minutes (e.g., 10 minutes) or on demand. Since the first-stage binary variables are known respect to the restoration time, the OR function can be quickly solved without additional delays to the restoration process. For instance, online generators can

be re-dispatched to provide sufficient amount of reserve to ensure system reliability in the case of contingencies. Should any contingencies occur or significant difference between estimated system parameters and real-time measurement data causes the non-convergence of OR optimization problem, the OP function needs a re-run based on the updated system states.

This sliding window approach is developed to improve the computational efficiency with a two-stage problem formulation. The first-stage problem contains integer variables and the second-stage problem is a MILP problem. The OP function solves the two-stage problem as a whole, while the OR function only solves the second-stage problem with the first-stage decisions fixed. This reduces the size and complexity of restoration in real-time applications. When contingencies occur, system topology changes and some of initially determined paths may become unavailable. As a result, the first-stage decisions need to be resolved by running the OP function. As shown in Fig. 1, when a major contingency occurs at t_{k+n+1} , the OP function is called. Note that at this moment, the size and computational time of the optimization problem will be considerably smaller than the original problem solved at t_{k+1} .

IV. RDSS PROBLEM FORMULATION

The proposed RDSS is modeled as a two-stage MILP problem. The first-stage problem decides generators start-up times and transmission lines energization sequences at the beginning of a restoration period. Given first-stage decisions, the second-stage problem determines optimal load pickup amount and location, dynamic reserve allocation, voltage profile, frequency behavior, and real and reactive power losses. In the second-stage problem, auxiliary variables and optimality cuts will be added to ensure the feasibility.

A. First-stage Optimization Problem

1) *Objective*: The objective of the first-stage problem is to maximize the total energy served by all generators through starting up more generators (or equivalently, to minimize negative energy supply), and minimize the value function of the second stage problem, $\varphi(u)$, as shown in (1). $\varphi(u)$ is explained in Section IV.B.

$$\text{Minimize} \left(- \sum_{t \in T} \sum_{i \in I} (P_g^{max,i} - P_{gstart}^i) u_{on}^{i,t} + \varphi(u) \right) \quad (1)$$

where, the binary decision variable $u_{on}^{i,t}$ is the status of generator i at restoration time t , with 0 meaning offline or starting up, and 1 meaning online. First-stage binary decisions are: $u_{start}^{i,t}$, $u_{on}^{i,t}$, $u_{bus}^{b,t}$, and $u_{line}^{nm,t}$. In (1), u is the vector of first-stage decisions.

2) *Constraints*: The first-stage problem includes three groups of constraints, and all decision variables satisfy $\forall t \in T, \forall i \in I, \forall nm \in K, \forall (n, m) \in B$, unless otherwise noted.

a) *Initial conditions*: Assuming a total blackout case occurs at $t = 0$, the initial conditions of the restoration problem are given in (1.1) and (1.2).

$$u_{start}^{i,t=0} = 0, u_{bus}^{b,t=0} = 0, u_{line}^{k,t=0} = 0 \quad (1.1)$$

$$u_{start}^{i,t=1} = 1 \quad \forall i \in I_{BSU} \quad (1.2)$$

b) *Generator start-up function*: The start-up characteristic of NBSUs is shown in (1.3), where integer variable t_{start}^i and parameter T_{start}^i represent start-up and cranking times. P_{start}^i is the cranking power of generator i . More details regarding the MILP representation of constraint (1.3) can be found in [11].

$$P_{gstart}^{i,t} = \begin{cases} 0 & 0 \leq t < t_{start}^i \\ P_{gstart}^i & t_{start}^i \leq t < (t_{start}^i + T_{start}^i) \end{cases} \quad (1.3)$$

Note that for $t \leq (t_{start}^i + T_{start}^i)$, generators' output power follow their start-up function, $P_{gstart}^{i,t}$. Whereas, for $t > (t_{start}^i + T_{start}^i)$, generators' scheduled power are determined in the second-stage problem, denoted by $P_g^{i,t}$.

c) *Start-up time constraints*: Generation unit i can go online only after its start-up time has elapsed, as shown in (1.4). The binary variable $u_{start}^{i,t}$ is 1 if unit i is starting up; otherwise is 0. The relationship between t_{start}^i and $u_{start}^{i,t}$ are shown in (1.5).

$$\sum_{t \in T} (1 - u_{on}^{i,t}) \geq \sum_{t \in T} (1 - u_{start}^{i,t}) + T_{start}^i \quad (1.4)$$

$$t_{start}^i = \sum_{t \in T} (1 - u_{start}^{i,t}) \quad (1.5)$$

d) *Buses and lines energization constraints*: The relationship of bus and line energization can be modeled as following: constraint (1.6) shows that NBSUs can be started after energizing their corresponding buses b_i ; constraints (1.7) and (1.8) show that if both connected buses are de-energized at restoration time t , then the line is de-energized at time t . Constraint (1.9) shows that if either bus is energized at t , the line can be energized at $t+1$ or remains de-energized. In radial energization, if a line is energized at $t+1$, buses at both ends of that line should be energized at $t+1$. Also, transmission lines should connect the energized buses to form a meshed network. In this case if a transmission line is energized at $t+1$, buses at both ends of the line should be energized at t .

$$u_{start}^{i,t} \leq u_{bus}^{b_i,t} \quad (1.6)$$

$$u_{line}^{nm,t} \leq u_{bus}^{n,t} \quad (1.7)$$

$$u_{line}^{nm,t} \leq u_{bus}^{m,t} \quad (1.8)$$

$$u_{line}^{nm,t+1} \leq (u_{bus}^{n,t} + u_{bus}^{m,t}) \quad (1.9)$$

B. Second-stage Optimization Problem

1) *Objective*: The objective of the second-stage problem is to minimize total unserved load plus a penalty function, as shown in (2). The penalty function includes two positive continuous variables, $q_+^{i,t}$ and $q_-^{i,t}$, which are fictitious reactive power sources installed at generation buses to ensure the feasibility of the optimization problem. These variables are

utilized for generating a set of optimality cuts to speed up the convergence of solution algorithm, as explained in section IV.

$$\varphi(u) = \text{Minimize} \left\{ \sum_{t \in T} \left(\sum_{l \in L} \alpha_l (P_{load}^{max,l,t} - P_{load}^{l,t}) + \sum_{i \in I} M(q_+^{i,t} + q_-^{i,t}) \right) \right\} \quad (2)$$

where α_l is each load's priority factor, $P_{load}^{max,l,t}$ shows the maximum restorable load, $P_{load}^{l,t}$ denotes the total restored load at load bus l and restoration time t .

2) *Constraints*: The second-stage problem includes five groups of constraints, and all decision variables satisfy $\forall t \in T, \forall i \in I, \forall nm \in K, \forall (n, m) \in B, \forall l \in L$. Also, the first-stage decision variables appeared in the second-stage constraints are considered as constant parameters and denoted with a hat sign.

a) *Power balance constraints*: Real and reactive power limits of each generator are shown in (2.1)-(2.2), where we replaced the generator capability curve with the rectangle constraints. With this assumption, it is guaranteed that any given active and reactive power can vary within the assigned range. Although conservative, it will dramatically decrease the complexity of the problem and computational time. Real and reactive power balance equations are built based on an undirected graph representation of the network, as presented in (2.3)-(2.4). Parameter $\hat{P}_{gstart}^{i,t}$ denotes the start-up power of generator i whose value is obtained from the first-stage problem.

$$P_g^{min,i} \hat{u}_{on}^{i,t} \leq P_g^{i,t} \leq P_g^{max,i} \hat{u}_{on}^{i,t} \quad (2.1)$$

$$Q_g^{min,i} \hat{u}_{on}^{i,t} \leq Q_g^{i,t} \leq Q_g^{max,i} \hat{u}_{on}^{i,t} \quad (2.2)$$

$$\sum_{i \in I} (P_g^{i,t} - \hat{P}_{gstart}^{i,t}) - \sum_{l \in L} P_{load}^{l,t} = \sum_{nm \in K} P_f^{nm,t} \quad (2.3)$$

$$\sum_{i \in I} (Q_g^{i,t} + q_+^{i,t} - q_-^{i,t}) - \sum_{l \in L} Q_{load}^{l,t} = \sum_{nm \in K} Q_f^{nm,t} \quad (2.4)$$

where, $P_f^{nm,t}$ and $Q_f^{nm,t}$ denote the real and reactive power flow of transmission line between buses n and m . The fictitious reactive power sources in the penalty function are also included in (2.4).

b) *Linearized AC load flow and transmission line constraints*: Linearized model of AC power flow equations through convex approximation are presented in (2.5)-(2.6). The piecewise linear approximation of cosine function using binary variables is shown in (2.7), where cosine function is divided into N_r equal segments and index $r = 0, \dots, N_r - 1$ denotes each segment. The linear function in each segment is determined through choosing appropriate values of $z^{nm,r}$ and $a^{nm,r}$ (as referred in [21]).

$$P_f^{nm,t} = (2V^{n,t} - 1)g_{nm} - (V^{n,t} + V^{m,t} + y^{nm,t} - 2)g_{nm} - b_{nm}\theta^{nm,t}, \quad n \neq m \quad (2.5)$$

$$Q_f^{nm,t} = -(2V^{n,t} - 1)(b_{nm} + b_{nm}^c) + (V^{n,t} + V^{m,t} + y^{nm,t} - 2)b_{nm} - g_{nm}\theta^{nm,t}, \quad n \neq m \quad (2.6)$$

$$y^{nm,t} = z^{nm,r}\theta^{nm,t} + a^{nm,r} \quad \forall (nm) \in K, r = 0, \dots, N_r - 1 \quad (2.7)$$

c) *Bus and line limit constraints*: Real and reactive power flows of de-energized transmission lines must be equal to zero, as shown in (2.8)-(2.9). Voltage magnitude of all energized buses should be maintained between 95% to 105% of nominal voltage in (2.10). Thermal limits of transmission lines are expressed in (2.11). Given the apparent power limitation of transmission line, \hat{S}^{nm} , one can calculate $\hat{P}^{nm} = \frac{g_{nm}}{g_{nm}^2 + b_{nm}^2} \hat{S}^{nm}$ [21].

$$-M\hat{u}_{line}^{nm,t} \leq P_f^{nm,t} \leq M\hat{u}_{line}^{nm,t} \quad (2.8)$$

$$-M\hat{u}_{line}^{nm,t} \leq Q_f^{nm,t} \leq M\hat{u}_{line}^{nm,t} \quad (2.9)$$

$$V^{min} \hat{u}_{bus}^{b,t} \leq V_{bus}^{b,t} \leq V^{max} \hat{u}_{bus}^{b,t} \quad (2.10)$$

$$P_f^{mn,t} + P_f^{nm,t} \leq \hat{P}^{nm} \quad (2.11)$$

d) *Real and reactive load constraints*: The static load model, namely ZIP model [22], is applied in this paper. The non-linear ZIP load model together with its linear equivalent is presented in (2.12) [15].

$$P_{load}^{max,l,t} \leq (\mu_p + \mu_I \frac{V^{b,t}}{V_0} + \mu_z (\frac{V^{b,t}}{V_0})^2) P_{load}^{l,V_0} \approx (\mu_p - \mu_z + \frac{V^{b,t}}{V_0} (\mu_I + 2\mu_z)) P_{load}^{l,V_0} \quad (2.12)$$

where, P_{load}^{l,V_0} represents real power demand at bus l and nominal voltage V_0 . Real and reactive loads can be restored only after energizing their respective buses, as shown in (2.13)-(2.14). And the reactive load pickup limit is shown in (2.15).

$$0 \leq P_{load}^{l,t} \leq P_{load}^{max,l,t} \hat{u}_{bus}^{b_l,t} \quad (2.13)$$

$$0 \leq Q_{load}^{l,t} \leq Q_{load}^{max,l,t} \hat{u}_{bus}^{b_l,t} \quad (2.14)$$

$$Q_{load}^{l,t} \leq P_{load}^{l,t} \tan(\arccos(pf_l)) \quad (2.15)$$

e) *Load pickup and dynamic reserve constraints*: Load pickup limit is modeled in (2.16), where ΔP_{max}^t is the system load pickup capability at restoration time t , and ΔP_{CLPU}^t is the impact of cold load. The load pickup capability can be estimated by having system inertia, governor ramp rate and dead band, and minimum allowable frequency dip [23], as expressed in (2.17). Where, \hat{R}_g (MW/s) and \hat{M}^t (MW.s/Hz) are constant parameters that can be calculated right after determining the first-stage decisions. Also, the impact of cold load pickup is calculated in (2.18) [16], where β_l denotes the cold load percentage of load bus l , and λ_l represents the additional power demand caused by cold load phenomenon.

$$\sum_{l \in L} P_{load}^{l,t+1} - \sum_{l \in L} P_{load}^{l,t} + \Delta P_{CLPU}^t \leq \Delta P_{max}^t \quad (2.16)$$

$$\Delta P_{max}^t \leq \sqrt{2\hat{R}_g^t \hat{M}^t (f_0 - f_{min} - f_{ab})} \quad (2.17)$$

$$\Delta P_{CLPU}^t = \sum_{l \in L_{CLPU}} \beta_l \lambda_l (P_{load}^{l,t+1} - P_{load}^{l,t}) \quad (2.18)$$

Also, there should be enough dynamic reserve to survive the frequency decay as a consequence of largest generation unit's trip. The dynamic reserve is composed of two parts, governor response of conventional generation units and loads with under-frequency load shedding relays, as shown in (2.19).

$$P_{reserve}^{dyn,t} \leq \sum_{l \in L_{sh}} P_{shed}^{l,t} + \sum_{i \in I} P_{reserve}^{dyn,i,t} \quad (2.19)$$

In (2.20), $P_{reserve}^{dyn,i,t}$ limits the maximum contribution of generator i to the total dynamic reserve at restoration time t . Constraint (2.21) represents that each generation unit's power level should be limited to maintain system reliability. In (2.22), it is assumed that less than 50% of dynamic reserve in a system should be devoted to the loads with under-frequency load shedding relays [5].

$$P_{reserve}^{dyn,i,t} \leq \min(\Delta P_{max}^{i,t}, P_g^{max,i} - P_g^{i,t}) \quad (2.20)$$

$$P_g^{i,t} \leq P_{reserve}^{dyn,t} - P_{reserve}^{dyn,i,t} \quad (2.21)$$

$$\sum_{l \in L_{sh}} P_{shed}^{l,t} \leq 0.5 P_{reserve}^{dyn,t} \quad (2.22)$$

C. Constraints After Contingency Occurrence

Assuming that a contingency occurs at $t = t_c$, the OP problem (1) should be re-solved to obtain a new restoration plan. At this time, a new set of initial conditions should be developed. However, the objective functions of the first and second-stage optimization problems remain unchanged. Also, the restoration time will be reset and $t \rightarrow t'$. The following conditions would occur after the contingency:

a) *Condition 1:* If generation unit i is on before the contingency and it has not been affected by the contingency, it will maintain its status in (3.1). The same initial conditions are applied to the transmission lines and buses in (3.2).

$$u_{on}^{i,t'=0} = u_{on}^{i,t_c} \quad \forall i \in I_{in} \quad (3.1)$$

$$u_{bus}^{b,t'=0} = u_{bus}^{b,t_c}, \quad u_{line}^{k,t'=0} = u_{line}^{k,t_c} \quad \forall b \in B_{in}, \quad k \in K_{in} \quad (3.2)$$

b) *Condition 2:* If generation unit i is in start-up period (i.e. $u_{start}^{i,t_c} = 1$) and it has not been affected by the contingency, it will continue its start-up process; however, the start-up constraint will be updated in (3.3). Where, \hat{t}_{start}^i is a constant parameter denoting the initial start-up time derived after running OP at $t = 0$.

$$P_{gstart}^{i,t'} = P_{gstart}^i \quad 0 \leq t' < T_{start}^i + \hat{t}_{start}^i - t_c \quad \forall i \in I_{in} \quad (3.3)$$

c) *Condition 3:* If generation unit i is off and $u_{start}^{i,t_c} = 0$, and it has not been affected by the contingency, it follows a normal start-up process as expressed in (1.3)–(1.5). Also, constraints (1.6)–(1.9) are applied to the unaffected de-energized buses/lines.

d) *Condition 4:* If generation unit i is on/off or in start-up process before the contingency happens, and it has been affected by the contingency, it will remain off until the end of outage time, denoted as T_o' in (3.4). This condition is applied to the energized/de-energized buses and lines.

$$u_{start}^{i,t'} = u_{on}^{i,t'} = 0, \quad u_{bus}^{b,t'} = 0, \quad u_{line}^{k,t'} = 0, \quad 0 \leq t' \leq T_o', \quad \forall b \in B_{out}, \quad k \in K_{out}, \quad i \in I_{out} \quad (3.4)$$

e) *Initial conditions for the second-stage problem:* System loads may also be affected partially or totally by the contingency. In (3.5), initial conditions of the active and reactive loads are set. However, if a load bus becomes de-energized after the contingency, its corresponding load value is forced to be zero in (3.6).

$$P_{load}^{l,t'=0} = P_{load}^{l,t_c}, \quad Q_{load}^{l,t'=0} = Q_{load}^{l,t_c} \quad \forall l \in B_{in} \quad (3.5)$$

$$P_{load}^{l,t'} = Q_{load}^{l,t'} = 0 \quad \forall t' \in T', \quad \forall l \in B_{out} \quad (3.6)$$

V. INTEGER L-SHAPED SOLUTION ALGORITHM

The integer L-shaped algorithm was introduced by Laporte and Louveaux [24] to tackle problems having binary first-stage decision variables and mixed-integer recourse. In this method, the first-stage problem can be solved using branch-and-cut algorithm and the second-stage problem is approximated by linear cuts. When a feasible first-stage solution is obtained, the second-stage problem is solved to generate an optimality cut to refine the approximation. Then, the first-stage problem is resolved with the generated optimality cut to obtain a new integer solution. This process iteratively continues until the optimal solution is found.

A. Algorithm Procedure

The restoration problem (1)–(2) can be represented as a general form of the following:

$$\text{Minimize } \{c^T x + Q(x)\}_{x \in \{0,1\}^n}$$

subject to:

$$\text{Constraints (1.1) – (1.9), (2.1) – (2.22)} \quad (4)$$

where x represents the first-stage decision variables and $Q(x)$ is the recourse function. Note that after the contingency at $t = t_c$, the constraints pertaining to the initial conditions of problem (4) should be updated to reflect the current state of the power grid, as expressed in section IV.C.

Let (5) be the relaxed master problem (RMP), the variable ϕ is estimated second-stage objective function for a given first-stage solution.

$$\text{Minimize } \{c^T x + \phi\}_{x \in [0,1]^n}$$

subject to:

$$\text{constraints (1.1) – (1.9)}$$

$$\text{integer L-shaped cuts}$$

$$\phi \geq LB \quad (5)$$

To solve the optimization problem (5), the integer L-shaped method employs the traditional branch and cut algorithm in the first-stage problem. The branch and cut procedure constructs a search tree consisting of nodes and branches. Those nodes connected to only one parent node and considered for branching are called pendant nodes. Pendant nodes in the search tree represent the sub-problems that should be processed until no more active nodes are available.

Having solved the RMP, those binary variables that did not get binary values become candidate for branching. The branching creates two pendant nodes representing two sub-problems that should be appended to the search tree. Whenever a binary solution is encountered, a lower bounding constraint on ϕ , called “optimality cut” is introduced. The general integer L-shaped optimality cut is defined in (6) [24].

$$\phi \geq (Q(x^v) - LB) \left(\sum_{i \in S^v} x_i - \sum_{i \notin S^v} x_i - |S^v| + 1 \right) + LB$$

$$v = 1, 2, 3, \dots, D \quad (6)$$

where, $S^v := \{i : x_i^v = 1\}$ is the index set of v^{th} feasible solution, and $|S^v|$ is the cardinality of S^v ; it gives the number of current first-stage decision variables with non-zero values. Also, LB is a global lower bound on $Q(x)$ (i.e. $Q(x) \geq LB$). Note that $\sum_{i \in S^v} x_i - \sum_{i \notin S^v} x_i$ is always less than or equal to the $|S^v|$. Let $W^v(x) = (\sum_{i \in S^v} x_i - \sum_{i \notin S^v} x_i - |S^v| + 1)$, if x_i is the v^{th} first-stage feasible solution (i.e. $x_i = x_i^v$), $W^v(x) = 1$ and the right hand side of (6) takes the value of $Q(x^v)$. Otherwise, $W^v(x) \leq 0$ and $\phi \geq LB + F$, where $F \leq 0$. This implies that the optimality cut (6) is tight at x_i^v and explicitly cuts off the current solution. In addition, this cut holds for all other feasible solutions. The proposed decomposition algorithm based on the integer L-shaped method can be summarized as follows:

Step 1) Set iteration count $D = 0$, the lower bounding constraint $LB = 0$. Set the best known solution (incumbent) $\bar{z} = \infty$. Construct a search tree whose root node is the relaxed master problem in (5).

Step 2) From the search tree, a pendant node is selected. If not exist, the algorithm is terminated and the best solution is printed. The algorithm stops when there are no more sub-problems for processing.

Step 3) Set $D = D + 1$, solve the RMP at current pendant node and let $z = c^T x^D + \phi^D$ be its optimal value with x^D and ϕ^D being the optimal solution. In fact, z holds the optimal solution of the current sub-problem at each iteration.

Step 3.1) If the current problem has no feasible solution or the solution is worse than the incumbent, $z \geq \bar{z}$, fathom the current node and go to step 2. That is, the process on this node is finished and no further branching is applied.

Step 3.2) If the current solution is not integer, create two new branches on fractional variables and append them to the list of pendant nodes and go to step 2. This step adds new pendant nodes to the search tree which need to be processed at next iterations.

Step 3.3) If the current solution is integer, compute the second-stage problem (2), let $z^D = c^T x^D + Q(x^D)$ and update

the new best solution $\bar{z} = \min\{\bar{z}, z^D\}$. This step intends to keep the current solution if it is the best found to date.

Step 4) If $\phi^D \geq Q(x^D)$, then fathom the current node and go to step 2. This condition implies that the x^D is an optimal solution. Thus, the process on this node should be terminated. If $\phi^D < Q(x^D)$, then generate an integer L-shaped cut (6), insert it into (5) and go to step 3.

B. Proposed Integer L-shaped Optimality Cut

The general form of the optimality cut presented in (6) introduces a relationship between the first-stage decision x and the second-stage objective function $Q(x)$. This cut yields a very promising result for the convergence time, given that the first-stage decision is feasible for the second-stage problem. However, when the first-stage solution is not feasible for the second-stage problem, the convergence time will increase remarkably. To cope with this problem, we propose a strong linear optimality cut based on the linearized form of AC power flow formulation presented in (2.6).

The proposed optimality cut is expressed in (7) showing that the reactive power balance should be held at each restoration time. The left hand side of the inequality constraint (7) controls the number of energized lines $u_{line}^{nm,t}$, by considering the number of online generators $u_{on}^{i,t}$, and total restored load $\hat{Q}_{load}^{tot,t}$. Indeed, the line charging current $\hat{Q}_{ch}^{nm,t}$ and reactive power loss $\hat{Q}_{loss}^{nm,t}$ vary with the number of energized transmission lines. Since at early phases of restoration process, only a few generators are online, causing a limited active/reactive load pickup capability and reactive power absorption capacity, the number of energized line should be restricted.

$$\sum_{nm \in K} (\hat{Q}_{ch}^{nm,t} - \hat{Q}_{loss}^{nm,t}) u_{line}^{nm,t} + \sum_{i \in I} \hat{Q}_g^{min,i} u_{on}^{i,t} \leq \hat{Q}_{load}^{tot,t} \quad (7)$$

where, $\hat{Q}_{ch}^{nm,t}$, $\hat{Q}_{loss}^{nm,t}$ and $\hat{Q}_{load}^{tot,t}$ are constant parameters that can be derived from the second-stage problem. Also, $\hat{Q}_g^{min,i}$ can be obtained from each generator manufacturer’s data sheet. The linearized forms of reactive power generated by the shunt elements of the equivalent π -model and reactive loss of transmission line nm can be computed in (8) and (9), respectively (note that $b_{nm} \leq 0$, and $b_{nm}^c \geq 0$).

$$\hat{Q}_{ch}^{nm,t} = 2b_{nm}^c (\hat{V}^{n,t} + \hat{V}^{m,t} - 1) \quad (8)$$

$$\hat{Q}_{loss}^{nm,t} = -2b_{nm} (1 - \hat{y}^{nm,t}) \quad (9)$$

VI. NUMERICAL RESULTS

To evaluate the adaptivity and computational efficiency of the proposed RDSS, we perform a case study on the IEEE-39 bus system. The restoration is assessed in a base case and in a contingency case. A complete blackout condition is assumed and one BSU (G10) and nine NBSUs (G1-G9) are participating in the restoration process. The generators’ characteristics and system load values and priorities are listed in Tables I and II. Each restoration time is assumed to be 10 minutes, which can be adjusted by system operators. Base

power is assumed to be 100 MW and the frequency nadir following a load pickup step must not exceed 59.6 Hz. Governors' dead band are assumed to be zero ($f_{db}=0$), cold loads are in buses 7, 26, and 31 with $\beta_l=20\%$, additional power demand $\lambda_l=1.5$, and loads are assumed to be dispatchable. The proposed RDSS with the integer L-shaped algorithm was implemented in C++ using the Concert Technology library of IBM ILOG CPLEX 12.6 [25]. We use Callback feature in CPLEX in which the second-stage problem is embedded and optimality cuts will be added to the master problem at each iteration. The advantage of this advanced computational feature is that it explores the entire search tree only once, which greatly reduces the computing time. All simulations were executed on a PC with Intel CoreTM i5 CPU @3.30 GHz and 8 GB RAM.

A. Restoration in the Base Case

We run the RDSS optimization problem for IEEE 39-bus system and the results are exhibited in Table III, where the first column shows the decisions by only solving the first-stage problem. When inserting these decisions into the second-stage problem, a large infeasibility penalty factor is resulted. Thus, the optimality cuts (6) and (7) are generated and added to first-stage problem to re-adjust the initial decisions. The second-column of Table III indicates the adjusted solution, which is feasible for both first and second-stage problems. One can see that without considering practical constraints for load pickup in the second stage, the generator start-up sequence becomes impractical to deploy.

In Fig. 2, a graphical representation of recovery process is depicted for $t = 11$ restoration time. The solid lines, representing the first-stage solution, show the transmission lines and buses that have been energized. It is clear from the figure that all generation units have their cranking paths established by that time. Whereas, the RDSS solution is shown by the dotted lines, where only two generators G7 and G9 have the established cranking paths and the restoration paths have altered significantly.

The RDSS restoration curve is plotted for entire restoration process and shown in Fig. 3. The load pickup process is started after restoration time 4 when the first load bus becomes energized, and is terminated after restoration time $t = 38$. System generation and load are balanced at all times, while voltage profiles are maintained within acceptable range, as shown in Fig. 4.

B. Restoration in the Contingency Case

In this case we study the response of the proposed RDSS to a major contingency during the restoration period. To this end, we assume that a contingency happens at $t = 11$ restoration time and the affected area is shaded and shown in Fig. 5. This contingency results in the trip of generation unit G9 together with the outage of the energized transmission lines (1-39), (3-4), (4-5), (4-14), (39-9), and (5-6). Also, we assume that transmission line (6-7) is out of service due to maintenance and repair.

TABLE I
GENERATORS' CHARACTERISTICS

Gen No.	$P_g^{min,i}$ (MW)	$P_g^{max,i}$ (MW)	$Q_g^{min,i}$ (MVar)	$Q_g^{max,i}$ (MVar)	P_{start}^i (MW)	Bus No.
1	0	570	-200	300	5	31
2	0	650	-250	300	7	32
3	0	630	-250	250	5	33
4	0	600	-220	300	8	34
5	0	650	-200	300	6	35
6	0	560	-200	200	6	36
7	0	560	-200	200	6	37
8	0	830	-300	300	7	38
9	0	1100	-400	500	8	39
10	0	250	-150	150	0	30

TABLE II
LOAD VALUES AND PRIORITIES

Bus	P_{load}^{max} (MW)	Priority	U/f relay	Bus	P_{load}^{max} (MW)	Priority	U/f relay
3	322	1	No	21	274	0.9	No
4	500	0.8	Yes	23	247	0.8	Yes
7	233	1	No	24	308	1	No
8	522	1	No	25	224	0.9	No
12	7.5	1	No	26	139	1	No
15	320	0.8	Yes	27	281	1	No
16	329	1	No	28	206	0.9	No
18	185	0.9	No	31	9.2	1	No
20	680	1	No	39	1100	1	No

TABLE III
GENERATORS' ON TIME (P.U.) IN DIFFERENT CASES

Generator No.	First-stage Solution	Normal Case RDSS Solution	Contingency Case RDSS Solution
G1	12	16	22
G2	13	18	20
G3	13	17	17
G4	14	18	18
G5	14	18	19
G6	14	18	18
G7	9	9	9
G8	11	16	16
G9	9	9	out of service
G10	2	2	2

In Fig. 5, the dotted lines show the RDSS decisions before the contingency and highlight the cranking paths of generators G1 and G2. However, this presents the initial RDSS solution assuming that all transmission lines and buses (or substations) remain in service during the restoration process. When a contingency occurs, the RDSS quickly adapts to the changing system conditions, and computes a new restoration solution. The RDSS initial solution ensures sufficient dynamic reserve during the transition, while the updated solution guarantees the availability of new restoration paths. As a result, the restoration process is robust and adaptive to system contingencies.

We then validate the restoration actions in power system simulation program (PSS/E) using time-domain simulation. Right before the contingency occurs, total system load is 380

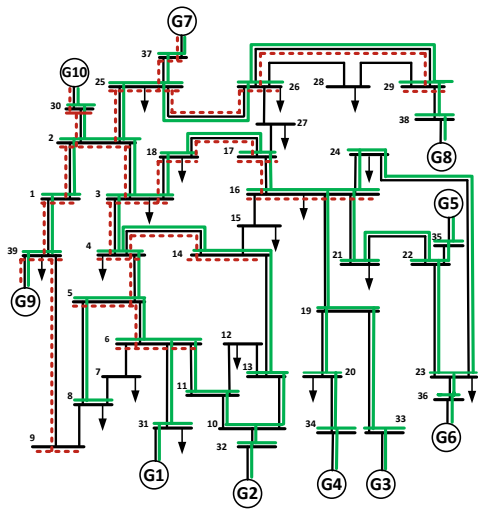


Fig. 2. Comparison between restoration paths, first-stage solution (solid line) and RDSS solution (dotted line) for $t = 11$ restoration time.

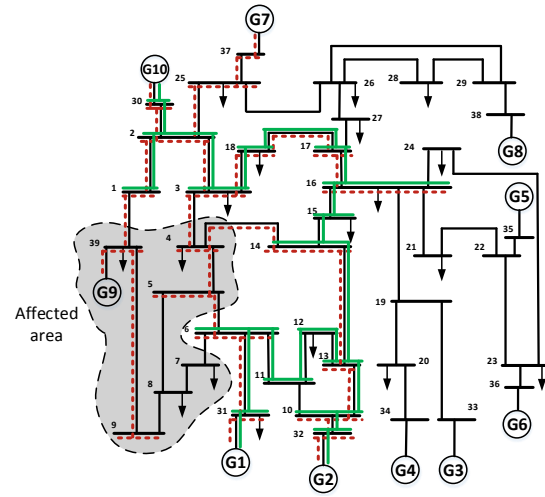


Fig. 5. Initial restoration paths for generators G1 and G2 (dotted lines), and the alternative restoration paths for generators G1 and G2 (solid lines) after the occurrence of a major contingency.

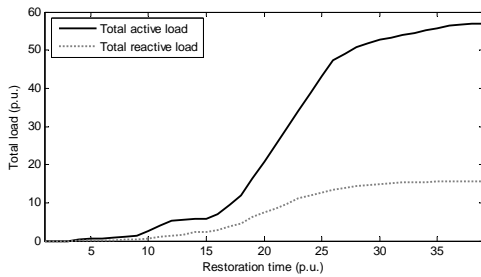


Fig. 3. Total active and reactive load pickup curves during the restoration.

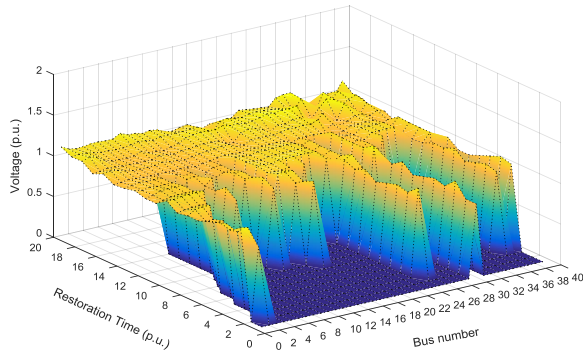


Fig. 4. Voltage profile before and after bus energization.

MW and generation units G10, G7 and G9 are responsible for load pickup. The maximum amount of dynamic reserve at this time is 230 MW. As shown in Fig. 6, after the trip of generation unit 9, the loss of 130 MW power supply is compensated by governor responses of two online generators, as well as load shedding at buses 4 and 39. The frequency nadir is well maintained above the minimum permissible frequency and the system survives under the contingent condition.

Then, the RDSS quickly generates a new solution representing the alternative restoration paths, as shown by the solid lines in Fig. 5 and listed in Table IV. Specifically, transmission lines (5-6) and (4-14) are in the cranking path of generation

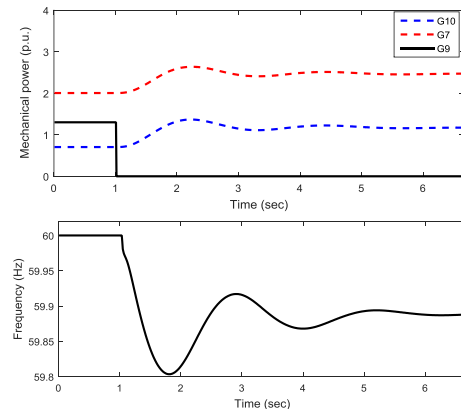


Fig. 6. Generators' mechanical power and system frequency traces after the contingency.

units G1 and G2. With the loss of these two lines, alternative paths are computed by the RDSS. The new generation start-up times can be found in Table III. One can observe that the start-up time of generation units G1, G2, and G5 have been changed under the new plan. Fig. 7 shows the restoration curve before and after contingency separated by the load shedding event at $t = 11$.

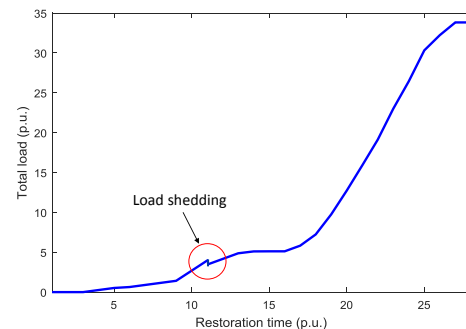


Fig. 7. Load restoration curve before and after contingency.

TABLE IV
CRANKING PATHS BEFORE AND AFTER THE CONTINGENCY

Gen. No.	Initial Cranking Paths (bus → bus)	Alternative Cranking Paths (bus → bus)
G1	(30-2) → (2-3) → (3-4) → (4-5) → (5-6) → (6-31)	(30-2) → (2-3) → (3-18) → (18-17) → (17-16) → (16-15) → (15-14) → (14-13) → (13-12) → (12-11) → (11-6) → (6-31)
G2	(30-2) → (2-3) → (3-4) → (4-14) → (14-13) → (13-10) → (10-32)	(30-2) → (2-3) → (3-18) → (18-17) → (17-16) → (16-15) → (15-14) → (14-13) → (13-10) → (10-32)

TABLE V
COMPARISON OF RDSS SOLUTION TIMES RESPECT TO THE TIME OF THE EXECUTION FOR IEEE 39-BUS SYSTEM WITH OPTIMALITY GAP = 1 %

Optimization problem	$t = 0$ (p.u.)	$t = 10$ (p.u.)	$t = 20$ (p.u.)
Without decomposition	1287 (sec)	968 (sec)	245 (sec)
Two-stage (RDSS-OP)	428 (sec)	315 (sec)	65 (sec)
RDSS-OR	68.8 (sec)	42.5 (sec)	15.2 (sec)

C. RDSS Performance

The RDSS can be used online in real-time operation due to its greatly improved computational performance. The improvement is two-folds, 1) the combinatorial problem is successfully decomposed into a two-stage formulation, which largely reduces the search of the entire feasibility region; 2) the computational burden is further reduced by the RDSS sliding-window framework, which only requires to solve the second-stage problem in real-time operation unless a contingency occurs. The performance of the two-stage decomposition RDSS framework is given at different restoration times in Table V, compared with the original problem without decomposition. Also, when the RDSS-OP is run at $t_c = 11$, right after the contingency, the convergence time becomes 286 s. Our RDSS clearly demonstrates superior performance that is suitable for real-time restoration.

VII. CONCLUSIONS

In this paper, we propose a novel adaptive decision support system namely RDSS to address the challenging online restoration problem. The proposed RDSS incorporates different phases of restoration into one holistic problem to guarantee the optimality throughout the entire restoration period. The complex combinatorial problem is decomposed into two-stage MILP formulation which can be solved using the integer L-shaped method. The two stages are then carried out in a sliding window framework to further improve the computational efficiency. Numerical results demonstrates the effectiveness of RDSS to quickly adapt to changing system conditions in an online restoration environment. RDSS is an important step toward a self-healing power grid and its implementation will reduce the recovery time while maintaining system security.

REFERENCES

[1] T. Zabaoui, L. A. Dessaint, I. Kamwa, "Preventive control approach for voltage stability improvement using voltage stability constrained optimal

power flow based on static line voltage stability indices," *IET Gener. Transm. Distrib.* vol. 8, no. 5, pp. 924-934, May 2014.

[2] U.S. Department of Energy Electricity Advisory Committee, "Smart grid enabler the new energy economy", Dec. 2008.

[3] M. Adibi, "Power system restoration: methodologies & implementation strategies," Wiley-IEEE Press, 2000.

[4] L. H. Fink, K. L. Liou, C.C. Liu, "From generic restoration actions to specific restoration strategies," *IEEE Trans. Power Syst.*, vol. 10, no. 2, pp. 745-752, May 1995.

[5] PJM Manual 36, System Restoration, June 2013, [online]. Available: <http://www.pjm.com>.

[6] ISO New England System Restoration Plan, [online]. Available: <http://www.iso-ne.com>.

[7] Y.T. Chou, C.W. Liu, Y.J. Wang, C.C. Wu, C.C. Lin, "Development of a black start decision supporting system for isolated power systems," *IEEE Trans. Power Syst.*, vol. 28, no. 3, pp. 2202-2210, Aug. 2013.

[8] M. M. Adibi, R. J. Kafka, and D. P. Milanicz, "Expert system requirements for power system restoration," *IEEE Trans. Power Syst.*, vol. 9, no. 3, pp. 1592-1598, Aug. 1994.

[9] M. M. Adibi and L. H. Fink, "Special considerations in power system restoration," *IEEE Trans. Power Syst.*, vol. 7, no. 4, pp. 1419-1427, Nov. 1992.

[10] Y. Hou, C.C. Liu, K. Sun, P. Zheng, S. Liu, and D. Mizumura, "Computation of milestones for decision support during system restoration," *IEEE Trans. Power Syst.*, vol. 26, no. 3, pp. 1399-1409, Aug. 2011.

[11] W. Sun, C.C. Liu, and L. Zhang, "Optimal generator start-up strategy for bulk power system restoration," *IEEE Trans. Power Syst.*, vol. 26, no. 3, pp. 1357-1366, Jun. 2011.

[12] C. Wang, V. Vittal, V. S. Kolluri, and S. Mandal, "PTDF-Based Automatic Restoration Path Selection," *IEEE Trans. Power Syst.*, vol. 25, no. 3, pp. 1686-1694, Aug. 2010.

[13] A. Stefanov, C.C. Liu, M. Sforna, M. Eremia, and R. Balaurescu, "Decision support for restoration of interconnected power systems using tie lines," *IET Gener. Transm. Distrib.*, vol. 9, no. 11, pp. 1006-1018, Aug. 2015.

[14] W. Liu, Z. Lin, F. Wen, and G. Ledwich, "A wide area monitoring system based load restoration method," *IEEE Trans. Power Syst.*, vol. 28, no. 2, pp. 2025-2034, May 2013.

[15] A. Gholami and F. Aminifar, "A hierarchical response-based approach to the load restoration problem," *IEEE Trans. Smart Grid*, to be published.

[16] Z. Qin, Y. Hou, C.C. Liu, Sh. Liu, W. Sun, "Coordinating generation and load pickup during load restoration with discrete load increments and reserve constraints," *IET Gener. Trans. Distrib.*, vol. 9, no. 15, pp. 2437-2446, Nov. 2015.

[17] A. M. El-Zonkoly, "Renewable energy sources for complete optimal power system black-start restoration," *IET Gener. Transm. Distrib.*, vol. 9, no. 6, pp. 531-539, Apr. 2015.

[18] C. Coffrin and P. V. Hentenryck, "Transmission system restoration with co-optimization of repairs, load pickups, and generation dispatch," *Int. J. Elect. Power Energy Syst.*, vol. 72, pp. 144-154, Nov. 2015.

[19] S.M. Mohammadi-Hosseininejad, A. Fereidunian, A. Shashavari, and H. Lesani, "A healer reinforcement approach to self-healing in smart grid by PHEVs parking lot allocation," *IEEE Trans. Ind. Inf.*, vol. 12, no. 6, pp. 2020-2030, Dec. 2016.

[20] M. Eriksson, M. Armendariz, O. O. Vasilenko, A. Saleem, and L. Nordstrom "Multiagent-based distribution automation solution for self-healing grids," *IEEE Trans. Ind. Electron.*, pp. 2620-2628, vol. 62, no. 4, Apr. 2015.

[21] P. A. Trodden, W. A. Bukhsh, A. Grothey, and K. I. M. McKinnon, "Optimization-based islanding of power networks using piecewise linear AC power flow," *IEEE Trans. Power Syst.*, vol. 29, no. 3, pp. 1212-1220, May 2014.

[22] A. Bokhari, A. Alkan, A. Sharma, R. Dogan, M. Diaz-Aguilo, F. de Len, D. Czarkowski, Z. Zabar, L. Birenbaum, A. Noel, and R. Uosef, "Experimental determination of the ZIP coefficients for modern residential, commercial, and industrial loads," *IEEE Trans. Power Del.*, vol. 29, no. 3, pp. 1372-1381, June 2014.

[23] H. Chvez, R. Baldick, and S. Sharma, "Governor rate-constrained OPF for primary frequency control adequacy," *IEEE Trans. Power Syst.*, vol. 29, no. 3, pp. 1473-1480, May 2014.

[24] G. Laporte, F.V. Louveaux, "The integer L-shaped method for stochastic integer programs with complete recourse," *Oper. Res. Lett.*, vol. 13, pp. 133-142, Apr. 1993.

[25] IBM ILOG CPLEX V 12.6, [online]. Available: <http://www.ibm.com/software/products/en/ibmilogcpleoptistud>.